ICAS-98-2,10,5

A98-31530

SUPERSONIC UNDEREXPANDED RECTANGULAR JET OSCILLATIONS: A COMPUTATIONAL STUDY

Sang Han
Department of Aerospace Engineering
The University of Kansas
Lawrence, Kansas 66045, USA
TEL: 785-864-4267 FAX: 785-864-3597
EMAIL: syhan@falcon.cc.ukans.edu

Ray R. Taghavi
Department of Aerospace Engineering
The University of Kansas
Lawrence, Kansas 66045, USA
TEL: 785-864-2973 FAX: 785-864-3597
EMAIL: rtaghavi@aerospace.ae.ukans.edu

Abstract

A computational study on the effects of nozzle exit geometry on the underexpanded supersonic jet evolution and comparison with experimental data is presented in this paper. The purpose of this study was to answer the following questions: (1) Can reasonable information about the unsteady flapping oscillations of underexpanded rectangular-supersonic jets be calculated by using the three-dimensional *Proteus* computer code? (2) What are the effects of nozzle exit geometry on mixing characteristics of supersonic jets? In this study, the supersonic jets emerging from the rectangular and notched nozzles are investigated for their mixing characteristics. The aspect ratio of these nozzles was 5.0. The computational analysis was conducted by running the three-dimensional *Proteus* code developed at NASA Lewis Research Center. The code solves the three-dimensional, Reynolds-averaged, unsteady, compressible Navier-Stokes equations in strong conservation law form. A structured grid system and an improved grid system produced by shock adaptive grid method was used for this study. The structured grid was used first and based on the results of calculations, the shock adaptive grid was generated and the code was run again with this new grid. The centerline distributions of axial velocity, static pressure, and mass flow rate are plotted and compared with experimental data along with the axial velocity and static pressure contour maps at the center planes. It is concluded that the three-dimensional *Proteus* code can be used to analyze the underexpanded supersonic rectangular jet mixing and flapping characteristics. It is also shown that the change of nozzle exit geometry strongly affects the jet mixing.

Introduction

Recent investigations in the supersonic rectangular jets are performed by several researchers computationally and experimentally.

The prediction of supersonic jet noise requires an ability to accurately simulate the mean flow jet structure and the interaction of jet under/overexpansion shocks with the turbulent mixing layer. To compute generalized supersonic jet flowfields with subsonic external streams, 3D codes which solve the Reynolds-Averaged Navier-Stokes equations in a time-asymptotic manner are required with the suitable turbulence models. In 1990, S.M. Dash et al.[1] used two 3D Reynolds-averaged Navier-Stokes(RNS) codes

in the study of the imperfectly expanded jets.

In 1994, G. Raman and E.J. Rice[2] examined experimentally the evolution of hydrodynamic instability modes, self-excited by harmonically related natural screech tones using a convergent rectangular nozzle with an aspect ratio of 9.63, producing a supersonic shock-containing jet. They observed the screech tone at the location where the growing instabilities interact with the shocks beyond the third shock cell.

In 1997, T. Huynh et al.[3] predicted the interaction, mixing characteristics, shock spacing, and shock strength of a twin-rectangular under-expanded jet at fully expanded Mach number of 1.55 using NPARC code. They showed that the computational results agree very well with the experimental data in the near field, but the shock strengths were under-estimated in the far field.

Y.B. Suzen and K.A. Hoffmann[4] used recently developed one-equation and two-equation turbulence models -- Baldwin-Barth one-equation model, Spalart-Allmaras one-equation model, and Menter's Zonal k-ω/ k-ε two-equation model -- to investigate their validation for analyzing supersonic jets computationally. They performed several modifications in model coefficients for the one-equation model and in compressibility correction for two-equation model for studying supersonic jet problems All their modifications in turbulence models showed improvements in the analysis of supersonic jets.

Woodruff et al.[5] evaluated the ability of two Navier-Stokes flow solvers -- ISAAC and PAB3D -- with several turbulence models to simulate the mean flow and turbulence properties of a supersonic jet plume. From their investigations they found that the two codes gave reasonably good results with the different turbulence models and the differences between two codes seemed to be greater than the differences between turbulence models.

G. Raman[6] summarized all aspects and issues relating to supersonic jet screech. In his paper he explained the source of screech tone propagating from the supersonic jets.

Mixing enhancement and noise reduction using streamwise vortices with tabs or trailing edge modifications of supersonic jets are studied by J.H. Kim et al.[7] They performed an experiment using an aspect ratio 3 rectangular nozzle with the design Mach number 2 to examine the effects of double-trailing edge modifications on mixing enhancement and thrust generated by the jet at the fully expanded Mach number of 1.75, 2.0, and 2.5. They showed that mixing enhancement could be achieved by using trailing edge modifications with minimal thrust loss in underexpanded flow regimes.

The primary purposes for this study are to investigate: (1) The capability of the three-dimensional *Proteus* code on the calculation of the three-dimensional unsteady characteristics of supersonic underexpanded jets, (2) The effects of nozzle exit geometry on mixing enhancement of supersonic jets, and (3) The validation of the shock adaptive grid system on the improvement of solution for supersonic underexpanded jets.

The supersonic jets with the rectangular nozzle and notched nozzle with aspect ratio of 5.0 and nozzle exit jet Mach number of 1.526 are analyzed with the plots of nozzle centerline distributions of axial velocity, static pressure, and mass flow rate. In addition, axial velocity and static pressure maps are also provided for studying supersonic jet flowfields. The computational results are also compared with experimental data when available.

Computational Fluid Dynamics (CFD)

For the study of the characteristics of supersonic jets, a computational code known as the three-dimensional *Proteus*[8],[9],[10] is used with grid systems produced from computer programs developed by the authors. Two turbulence models -- Baldwin-Lomax and Chien k-ε turbulence models -- are used for the calculations.

The code uses the three-dimensional compressible full Navier-Stokes equations in strong conservation law form using vector notation in Cartesian coordinates as the governing equations. For turbulent flow the equations are in the Reynolds time-averaged form of the Navier-Stokes equations with density fluctuation neglected. The governing equations are solved by marching in time from the given initial conditions using finite difference techniques, which is the generalized scheme of Beam and Warming.

Several options of boundary conditions, which are treated implicitly, are available in the code. These boundary conditions are used in the code after being linearized.

The governing equations are solved by an

alternating direction implicit (ADI) method, which is used with the appropriate factorization approach, with the boundary conditions specified for every computational domain boundaries; $\xi = 0$ and 1, $\eta = 0$ and 1, and $\zeta = 0$ and 1 planes.

In high Reynolds number flows the odd-even decoupling produced from the use of second order central differencing for the inviscid terms leads oscillations. Artificial viscosity is normally added to the solution algorithm to suppress high frequency instabilities, which occurs in a phenomena such as shock waves when they are captured by the finite difference algorithm. In the process of the execution, this artificial viscosity is applied to the computation. The code has two artificial viscosity options; a constant coefficient model[11] and the nonlinear coefficient model[12].

The constant coefficient artificial viscosity model of Steger[11] has both explicit and implicit artificial viscosities. The standard explicit smoothing uses fourth order differences, and damps the high frequency nonlinear instabilities. Also second order explicit smoothing is provided in the code, which gives more smoothing than fourth-order smoothing but has a larger error. The implicit smoothing is second order difference and extends the linear stability bound of the fourth order explicit smoothing. The nonlinear coefficient artificial viscosity model is strictly explicit.

The explicit and implicit artificial viscosities are applied in the computation algorithm, which is added in the solution procedure of ADI method.

The artificial damping can be controlled by adjusting artificial viscosity coefficients -- $\varepsilon_E^{(2)}$ for the second-order and $\varepsilon_E^{(4)}$ for the fourth-order explicit artificial viscosity; ε_I for the implicit artificial viscosity -- according to the problems and solutions.

Nozzle Configuration and Grid Generation

One effective method for passive excitation of supersonic jets is varying the nozzle exit plane shape.[13] These nozzle exit shapes are investigated as effective configurations for the mixing enhancement of supersonic jets.

The nozzles used in this study were convergent rectangular and notched rectangular shown in Figures 1 and 2 respectively. Nozzle dimensions are shown in Table I. Experimental studies using the above nozzles have been carried out by the previous researchers[3],[14],[15] and their results will be used for code validation.

Because of the three dimensional nature of the flow, full three-dimensional computational domains are used for both cases as shown in Figures 3 and 4.

The computational grid systems for this study are as shown in Figures 5 and 6 using the shock adaptive grid generator. The initial computations are executed with the rectangular structured grid systems, which have the grid size of 61x53x77 (248,941 grid points). After the initial computations, the shock adaptive grid generator is applied to the results of initial computations. The shock adaptive grid generator locates shocks from the initial computational results. The resulting shock adaptive grid systems are generated at 20% packing rate with nozzle centerline shock locations as shown in Figures 5 and 6 for the rectangular nozzle and the notched nozzle respectively. The shock adaptive grid system has grid sizes as follows;

a) Rectangular nozzle: 148x53x77
b) Notched nozzle: 131x53x77

The computations are executed using shock adaptive grid systems for the final computational results.

Boundary Conditions

Base boundary conditions for both cases are selected such that the boundaries except at nozzle exit and nozzle wall have zero gradient of pressure and velocities.[16] In addition, nozzle exit plane has design values for pressure, temperature, and velocity as follows with a choked condition at the nozzle exit:

Reference Condition:

Mach number	=	1.526
Temperature	=	249.85 K
Density	=	1.4138668 kg/m^3
Reference length	=	0.006 m

Boundary Condition:

ξ=0: Nozzle exit; p = 2.014, u = 1.0, v = w = 0.0
Nozzle wall; No-slip adiabatic wall
Outside; Subsonic inflow with zero gradient
ξ=1: Supersonic outflow with zero gradient

η=0,1: Subsonic outflow with zero gradient
ζ=0,1: Subsonic outflow with zero gradient

For both cases, the average residual in the order of 10^{-6} is used as the convergence guide and a time step with CFL number of 0.1 is used for a stable convergence.

In addition to the boundary conditions, artificial damping is applied to both supersonic computations with the following fourth-order explicit and second-order implicit artificial viscosities using a constant coefficient model of Steger[11]:

4^{th}-order explicit; $\varepsilon_E^{(4)} = 0.50$
2^{nd}-order implicit; $\varepsilon_I = 1.00$

Results and Discussions

Free Jet from Rectangular Nozzle

The computational analysis for the supersonic jet from the rectangular nozzle are introduced in terms of the nozzle centerline static pressure distribution, nozzle centerline axial velocity distribution, and mass flow rate distribution in the axial direction. In addition, contour maps of static pressure and axial velocity are presented with phase changing plots for better understanding of the unsteady oscillations.

In Figure 7, the nozzle centerline static pressure distributions are normalized using atmospheric pressure. In this plot, the axial distance is normalized with the nozzle height. The normalized axial distance is used throughout this study as standard independent axis. The experimental data[17] are also plotted in the above figure for the comparison purposes. It is shown in the plot that the computational solution agrees very well with the experimental data up to the third shock cell in terms of shock strength and shock spacing. After the third shock cell, the comparison can not be made. This is because the experimental results represent the mean flow data but the computational data are instantaneous values at a certain phase of flapping oscillation.

In Figure 8, the normalized mass flow rate distribution in the axial direction for the rectangular nozzle is included. Two available experimental data points[18] are also included in the plot. We can see from this figure that the code calculates the trend of a mass flow rate similar to the experimental data, which has the increasing trend as expected. The mass flow rate after the second shock cell ($x \geq 5.0h$, where flapping starts) should be presented with accumulated mass flow rate during one flapping oscillation period because the mixing is achieved by flapping oscillation disturbing quiescent air in rectangular supersonic free jet. The mixing area can be defined as the area occupied by the amplitude of jet flapping oscillation. The jet spreading phenomena also can be explained with this oscillation of the jet, which continuously extends the mixing area as time marches.

In Figure 9 a series of axial velocity contour maps at the center plane viewed from nozzle large and small dimensions for the rectangular jet are shown. Each figure is obtained with the phase interval of 45° (time step interval of about 1.7×10^{-5} second). In the large dimensional view, two shock cells are clearly visible. The jet shows a pumping motion described by the potential core being expanded and contracted alternatively as time marches. This phenomenon is also shown in Figures 9.f through 9.j for the axial velocity contour maps taken at the center plane viewed from nozzle small dimension, which clearly show flapping oscillation of the jet with frames at 45° phase difference. In addition, it is shown in this figure that the low pressure fields reside alternatively at each side of the jet and travel with the jet in the downstream direction as time elapses.

Figure 10 presents the rectangular jet oscillations using frames with 45° phase difference in terms of static pressure at the center plane viewed from large and small nozzle dimensions. It is seen in these figures that almost symmetric contours in the flowfield are investigated.

Similar phenomenon can be found in Figures 10.f through 10.j, which shows static pressure contour maps for the jet flapping oscillation at the center plane viewed from nozzle small dimension.

The frequency of the flapping oscillations from the experimental measurements is about 7400Hz.[17] From the computations, for the case of the rectangular nozzle, the frequency of the flapping oscillation is calculated to be about 7500Hz, which agrees very well with experimental results. We also see from Figures 9 and 10 that jet centerline location in the axial direction starts changing after the second shock cell because of the nature of two-dimensional flapping oscillations. In

the computations using the three-dimensional *Proteus* code, one iteration captures an image at one instant of time as the flapping oscillation progresses.

From the above figure, it is also examined that the acoustic waves are propagating out from the location of the third shock cell and moving upstream. These acoustic waves cause the screech tones and flapping oscillations of the underexpanded supersonic jets. The screech tone source is at the third shock cell as already reported in the literature[6].

Free Jet from Notched Nozzle

The supersonic rectangular jet from a 45° notched nozzle is analyzed computationally and the results are presented in this section.

In Figure 8, the mass flow rate distribution in the axial direction for the notched nozzle is also shown along with the case of the rectangular jet. We can see similar behavior of the mass flow enhancement in both cases. However, the direct comparison between two cases is not recommended because the base reference mass flow rates at the nozzle exit are different for each case.

Figures 11.a through 11.e show a series of axial velocity contour maps at the center plane viewed from the nozzle large dimension for flapping motion of the free jet from the notched nozzle. Each frame has the phase difference of 45° (time step interval of about 4.2×10^{-5} second). We can see the flapping oscillations in the direction of nozzle large dimension due to the effect of notch shape in the nozzle exit. This oscillation frequency was calculated to be about 3000Hz. This phenomena may be interpreted into the jet spreading characteristics of rectangular jet. Along with the flapping oscillation of the jet viewed from the large dimension, there is a pumping motion visible in the small dimension, as shown in Figures 11.f through 11.j. The pumping is described by the fact that a portion of the potential core coming out from notch is expanded and contracted alternatively, is found as time marches.

In addition, it is found from Figures 11.f through 11.j that the jet spreads out rapidly from the beginning of the notch, which explains the jet spreading characteristics of the notched rectangular jets. Also we can see the symmetry in axial velocity contours.

Figures 12.a through 12.e represent a half cycle of the jet oscillation process for the notched nozzle using frames with 45° phase difference in terms of static pressure at the center plane viewed from nozzle large dimension. We can see in these figures that two shock cells are clearly visible. Another fact which is clear from the above figure is that high and low pressure contours are located side by side across nozzle centerline, which makes the jet to flap. Thus we can confirm that the notch exit shape affects the supersonic jet flowfield in terms of mixing and jet spreading. Acoustic waves, which are found usually in static pressure contour maps at the center plane from nozzle small dimension for other cases, are shown in this large dimension static pressure maps of Figures 12.a through 12.e. This ensures that the flapping oscillation in the direction of nozzle large dimension generates acoustic waves in the same direction.

A series of 45° phase frames for static pressure contour maps for half cycle of jet evolving motion process at the center plane from nozzle small dimension are shown in Figures 12.f through 12.j. We can see from the figure that the jet flowfield shows symmetric static pressure contours.

Additionally, from Figures 9 and 11 we can see that the potential core for the notched nozzle case has smaller area than for the rectangular nozzle case. Also it is found that the jet height is much larger for notched nozzle case than for the rectangular nozzle case.

Conclusions

The three-dimensional *Proteus* code was successfully used as a computational tool to study underexpanded supersonic jet oscillations.

The three-dimensional, unsteady characteristics of rectangular jets such as flapping and spanwise oscillations, and pumping motion are well simulated with the advantage of unsteady capability of the code. The frequency of flapping oscillation for the case of the rectangular nozzle, was computed to be about 7500Hz, which is very comparable with experimental result of 7400Hz. Also, acoustic wave radiation was well simulated.

Shock adaptive grid technique improved the results of the three-dimensional *Proteus* code for the analysis of underexpanded supersonic free jets.

The change in the nozzle exit geometry had major effects on jet spreading, spanwise oscillations, flapping oscillations, and pumping motion of supersonic free

jets.

Acknowledgments

The authors' appreciation goes to Dr. Charles E. Towne from NASA Lewis Research Center for providing the three-dimensional *Proteus* code and his help in running the code.

References

(1) Dash, S.M., N. Sinha, B.J. York, and R.A. Lee, *"Progress in the Development of Advanced Computational Models for the Analysis of Generalized Supersonic Jet Flowfields,"* AIAA Paper 90-3915, October 1990.

(2) Raman, Ganesh and E.J. Rice, *"Instability Modes Excited by Natural Screech Tones in a Supersonic Rectangular Jet,"* Physics of Fluids, Vol.6 No.12, pp.3999-4008, December 1994.

(3) Huynh, T., R. Taghavi, and G. Raman, *"Computational Study of Twin Supersonic Jet Interaction,"* AIAA Paper 97-2285, June 1997.

(4) Suzen, Yildirim B. and K.A. Hoffman, *"Investigation of Supersonic Jet Exhaust Flow by One-and Two-Equation Turbulence Models,"* AIAA Paper 98-0322, January 1998.

(5) Woodruff, S.L., J.M. Seiner, M.Y. Hussaini, and G. Erlebacher, *"Evaluation of Turbulence-Model Performance as Applied to Jet-Noise Prediction,"* AIAA Paper 98-0083, January 1998.

(6) Raman, Ganesh, *"Advances in Understanding Supersonic Jet Screech,"* AIAA Paper 98-0279, January 1998.

(7) Kim, J.H., M. Samimy, and W.R. Erskine, *"Mixing Enhancement with Minimal Thrust Loss in a High Speed Rectangular Jet,"* AIAA Paper 98-0696, January 1998.

(8) Towne, C.E., J.R. Schwab, and T.T. Bui, *"Proteus Three-Dimensional Navier-Stokes Computer Code-Version 1.0; Volume 1-Analysis Description,"* NASA TM-106337, 1993.

(9) Towne, C.E., J.R. Schwab, and T.T. Bui, *"Proteus Three-Dimensional Navier-Stokes Computer Code-Version 1.0; Volume 2-User's Guide,"* NASA TM-106340, 1993.

(10) Towne, C.E., J.R. Schwab, and T.T. Bui, *"Proteus Three-Dimensional Navier-Stokes Computer Code-Version 1.0; Volume 3-Programmer's Reference,"* NASA TM-106341, 1993.

(11) Steger, J.L., *"Implicit Finite-Difference Simulation of Flow about Arbitrary Two-Dimensional Geometries,"* AIAA Journal, Vol. 16 No.7, pp. 679-686, 1978.

(12) Jameson, A., W. Schmidt, and E. Turkel, *"Numerical Solutions of the Euler Equations by Finite Volume Methods Using Runge-Kutta Time-Stepping Schemes,"* AIAA Paper 81-1259, 1981.

(13) Wlezien, R.W. and V. Kibens, *"Passive Control of Jets with Indeterminate Origins,"* AIAA Journal, Vol.24 No.8, pp. 1263-1270, August 1986.

(14) Sherwood, Thomas S., *"Subsonic Rectangular Jets with Swirling Shear Layers,"* M.S. Thesis, The University of Kansas, 1995.

(15) Taghavi, Ray and G. Raman, *"Twin Rectangular Supersonic Jet Interaction,"* 33rd AIAA/ASME/SAE/ASEE Joint Propulsion Conference and Exhibit, Seattle, Washington, July 6-9, 1997.

(16) McGuirk, J.J. and W. Rodi, *"The Calculation of Three-Dimensional Turbulent Free Jets,"* Turbulent Shear Flows, Vol.1, pp. 71-83, April 1977.

(17) Raman, Ganesh, *"Cessation of Screech in Underexpanded Jets,"* AIAA Paper 96-1719, 1996.

(18) Frank, Jason E., *"Experimental Investigation of the Effect of Swirl on Mixing Enhancement of Supersonic Rectangular Jets,"* M.S. Thesis, The University of Kansas, December 1994.

Table I. Nozzle geometric dimensions.

	Unit: mm
h : Nozzle height	7.270
L : Nozzle length	225.806
t : Nozzle wall thickness	0.635
w : Nozzle width	31.270
Aspect Ratio	5.000
For the notched nozzle	
ϕ : Notch half angle	45°

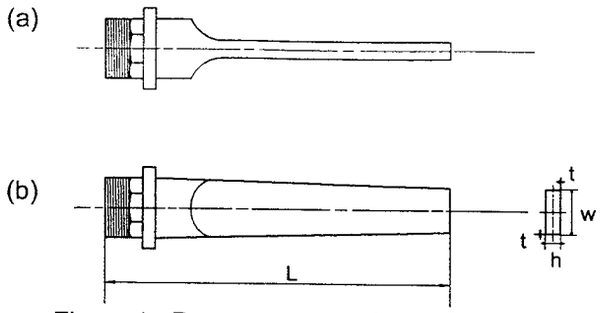

Figure 1. Rectangular nozzle configuration. (a) Side view, (b) Top view

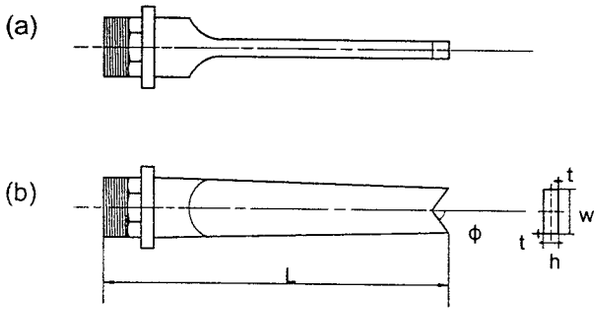

Figure 2. Notched nozzle configuration. (a) Side view, (b) Top view

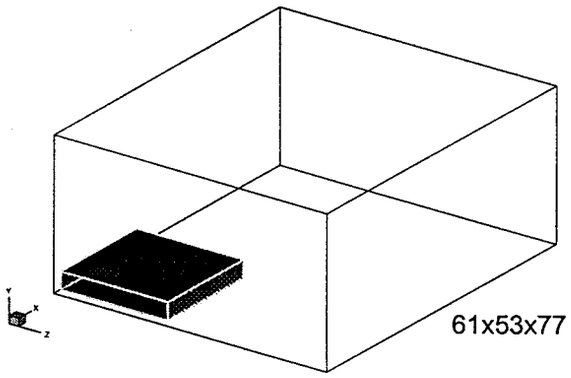

Figure 3. Computational domain for rectangular nozzle.

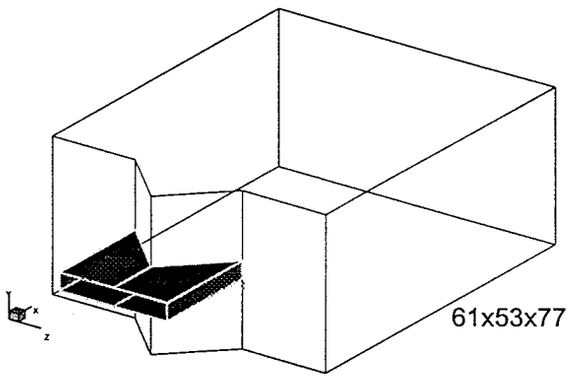

Figure 4. Computational domain for notched nozzle.

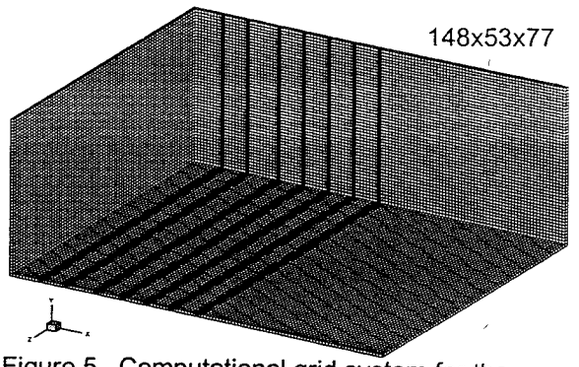

Figure 5. Computational grid system for the rectangular nozzle.

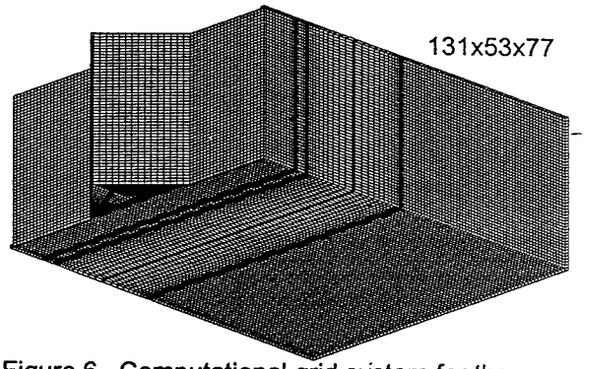

Figure 6. Computational grid system for the notched nozzle.

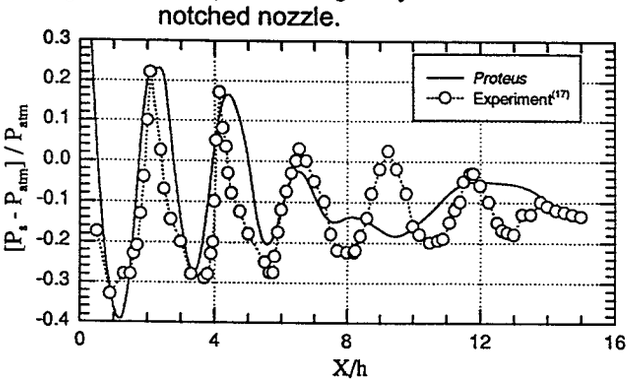

Figure 7. Nozzle centerline static pressure distribution in the axial direction for the rectangular nozzle.(M_j=1.526)

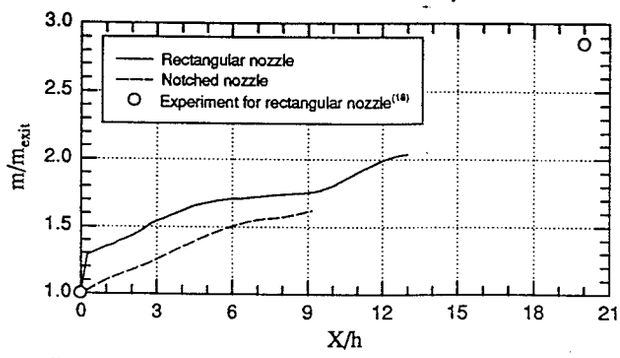

Figure 8. Comparison of mass flow rate distributions in the axial direction. (M_j=1.526)

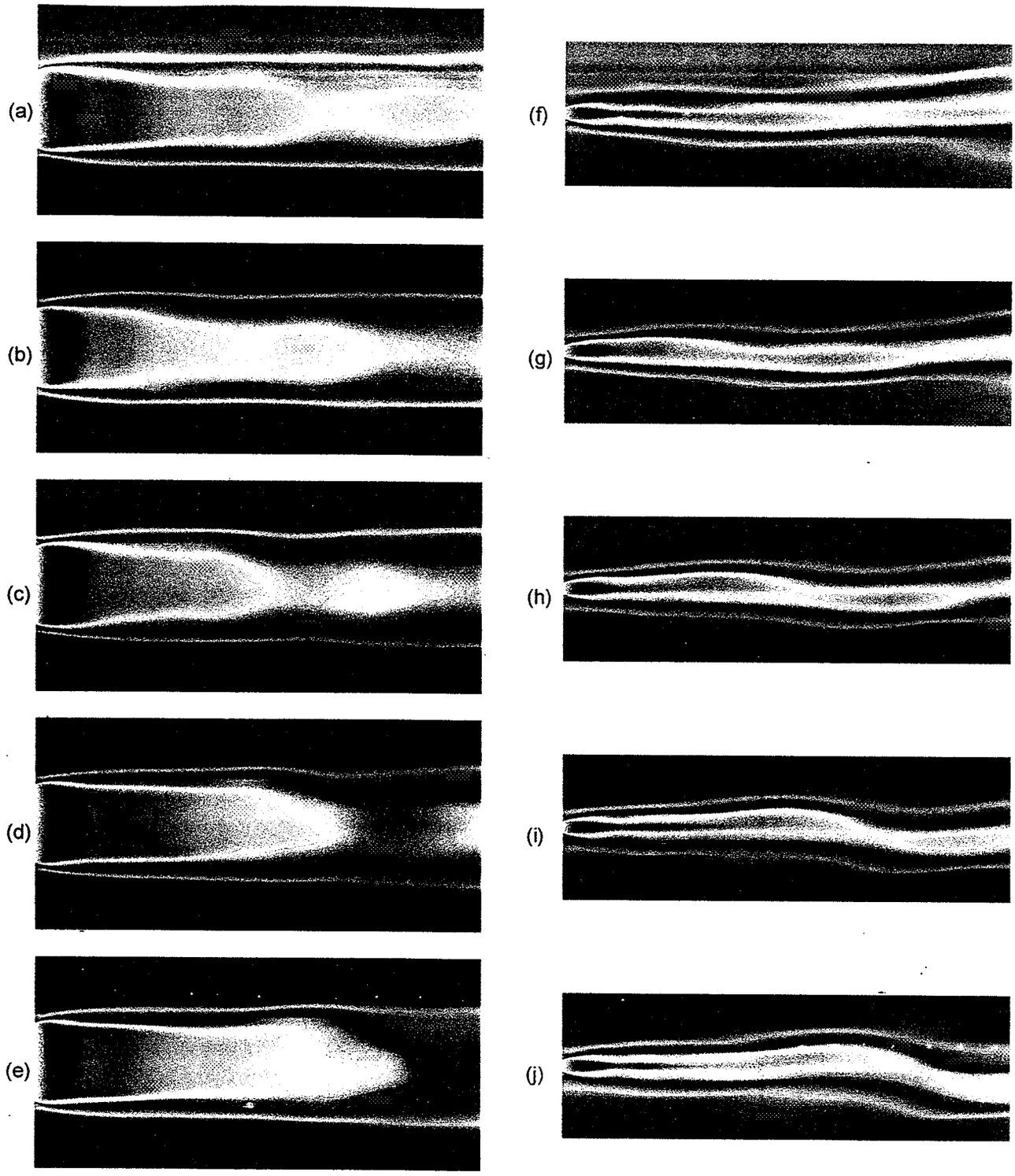

Figure 9. The rectangular jet oscillations at the center plane represented by axial velocity maps. Phase difference from frame to frame is 45°. Parts (a)-(e) represent views of half a cycle from nozzle large dimension. Parts (f)-(j) represent views of half a cycle from nozzle small dimension. (M_j=1.526)

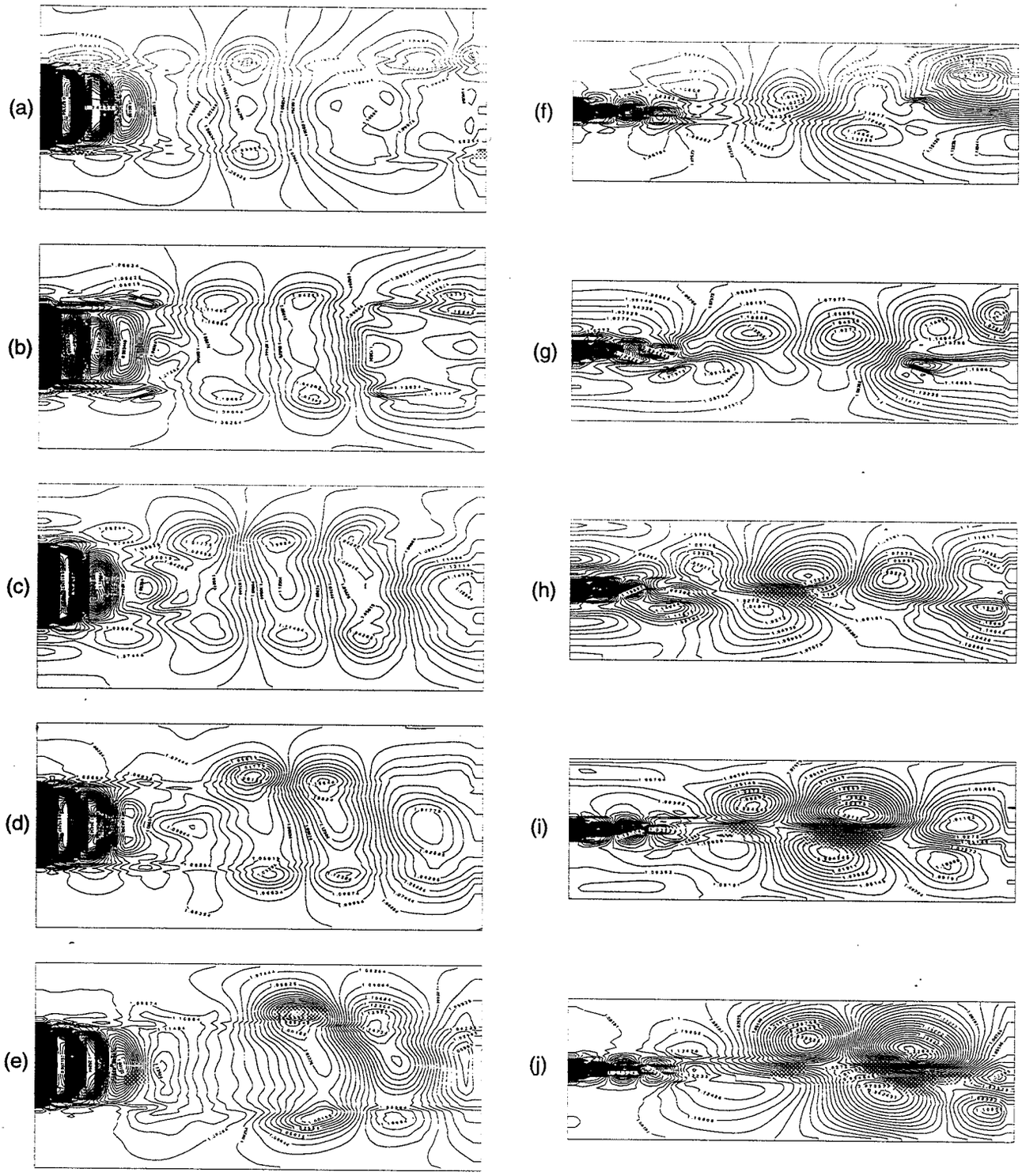

Figure 10. The rectangular jet oscillations at the center plane represented by static pressure maps. Phase difference from frame to frame is 45°. Parts (a)-(e) represent views of half a cycle from nozzle large dimension. Parts (f)-(j) represent views of half a cycle from nozzle small dimension. (M_j=1.526)

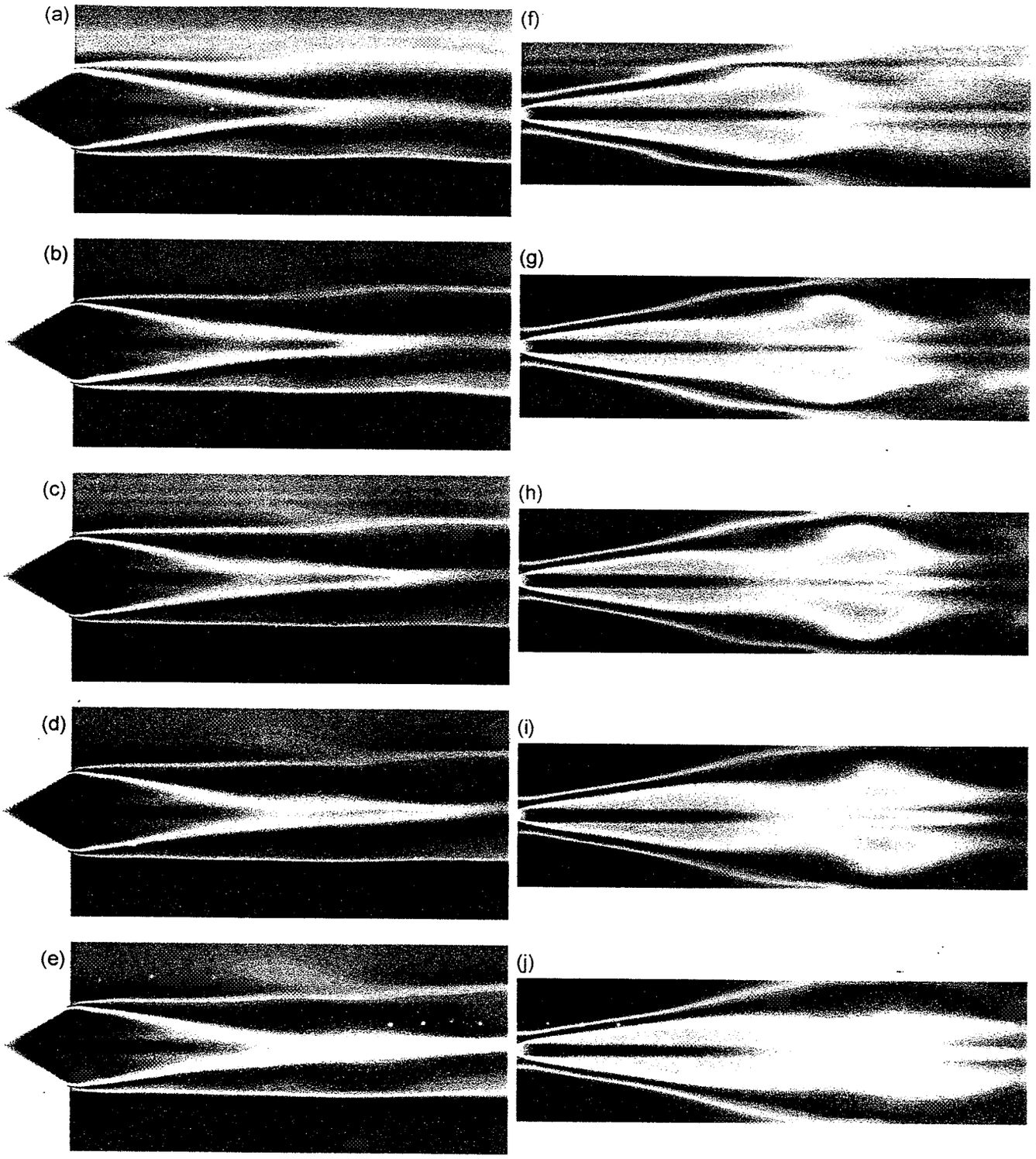

Figure 11. The jet oscillations at the center plane represented by axial velocity maps for the NOTCHED nozzle. Phase difference from frame to frame is 45°. Parts (a)-(e) represent views of half a cycle from nozzle large dimension. Parts (f)-(j) represent views of half a cycle from nozzle small dimension. (M_j=1.526)

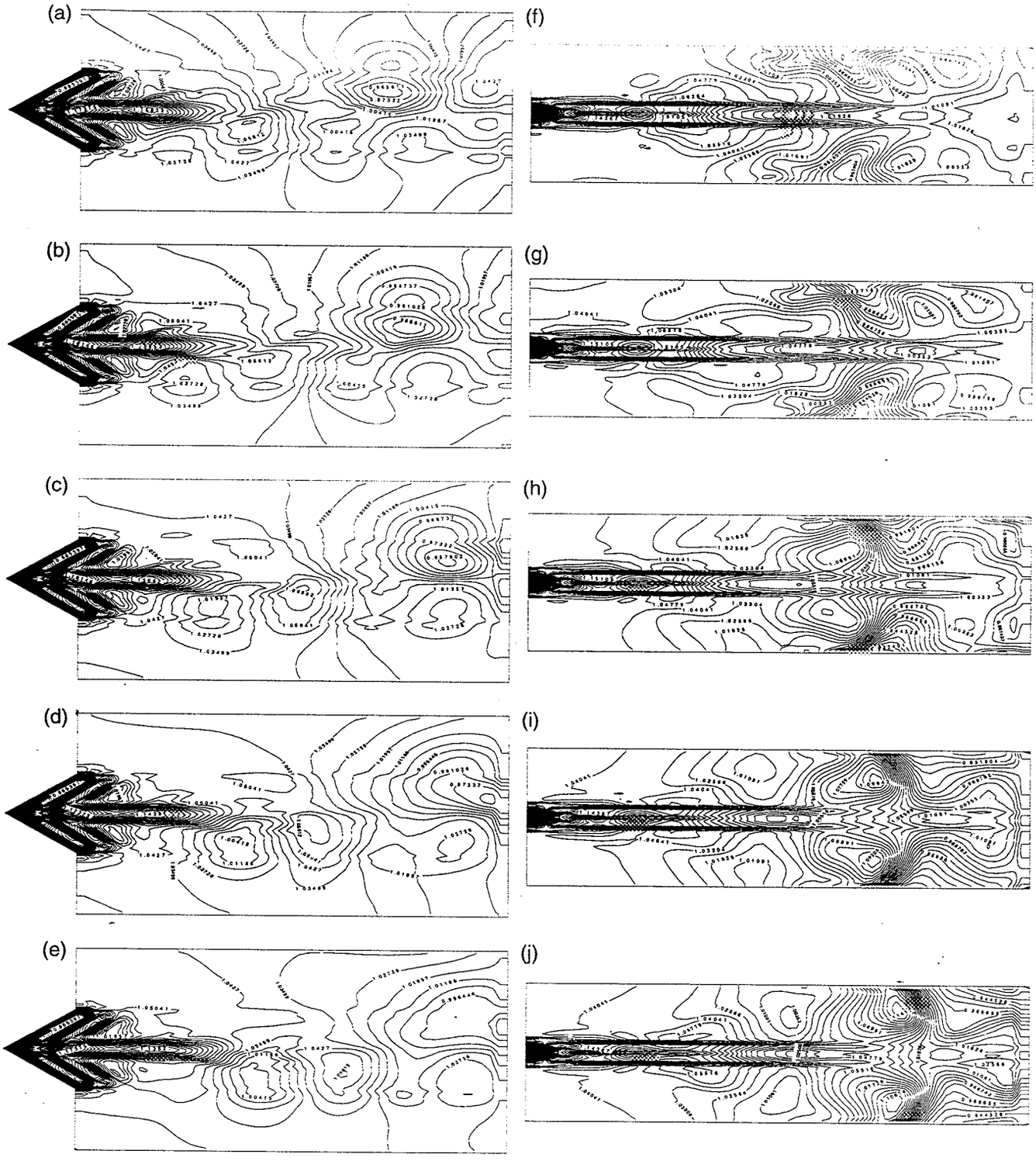

Figure 12. The jet oscillations at the center plane represented by static pressure maps for the **NOTCHED** nozzle. Phase difference from frame to frame is 45°. Parts (a)-(e) represent views of half a cycle from nozzle large dimension. Parts (f)-(j) represent views of half a cycle from nozzle small dimension. (M_j=1.526)